Updated Equipotential Shapes of Jupiter and Saturn Using Juno and Cassini Grand Finale Gravity Science Measurements

Buccino, Dustin R ; Helled, Ravit ; Parisi, Marzia ; Hubbard, William B ; Folkner, William M

Abstract: A commonly used shape model for the giant plants of Jupiter and Saturn is an oblate ellipsoid, a simplified model of the equipotential shape. The ellipsoidal shape models were originally derived from radio occultation data and gravity data after the Voyager flybys in 1979. Through precise Doppler tracking of NASA's Juno and Cassini spacecraft telecommunications links, zonal coefficients in a spherical harmonic expansion of the gravity field of Jupiter and Saturn have been resolved to degree 10, including the detection of nonzero odd zonal harmonics, which have been interpreted as differential rotation in the atmosphere for both planets. In this work, we construct the equipotential surfaces of Jupiter and Saturn using the recently measured gravity fields determined by Juno through perijove 8 and Cassini through end of mission. For both planets, even zonal harmonics dominate the equipotential shape, differing from the reference ellipsoid up to 32 km at Jupiter and 125 km at Saturn in the midlatitude regions. Saturn's internal rotation period estimated with ring seismology produces a shape that is fully consistent with the Pioneer and Voyager radio occultation measurements, and Jupiter's shape is fully consistent with the Pioneer and Voyager radio occultation measurements. With current equipotential theory, the recent analysis of the depth of the deep zonal flow on Jupiter and Saturn cannot fully be explained by the shape from current radio occultation measurements; additional occultation measurements and reanalysis of the Pioneer and Voyager radio occultations and will be useful for further constraining the shape of the planets.

DOI: https://doi.org/10.1029/2019je006354

JGR Planets

RESEARCH ARTICLE
10.1029/2019JE006354

Special Section:
Jupiter Midway Through the Juno Mission

Updated Equipotential Shapes of Jupiter and Saturn Using Juno and Cassini Grand Finale Gravity Science Measurements

Dustin R. Buccino[1], Ravit Helled[2], Marzia Parisi[1], William B. Hubbard[3], and William M. Folkner[1]

[1]Jet Propulsion Laboratory, California Institute of Technology, Pasadena, CA, USA, [2]Institute for Computational Science, University of Zurich, Zurich, Switzerland, [3]Lunar and Planetary Laboratory, University of Arizona, Tucson, AZ, USA

Key Points:
- Equipotential shape models for Jupiter and Saturn are derived from zonal spherical harmonic coefficients measured by Juno and Cassini
- Saturn's rotation rate measured by ring seismology is fully consistent with the radio occultation measurements of the shape
- The models are provided for general use in an accompanying dataset in commonly used formats

Correspondence to:
D. R. Buccino,
dustin.r.buccino@jpl.nasa.gov

Citation:
Buccino, D. R., Helled, R., Parisi, M., Hubbard, W. B., & Folkner, W. M. (2020). Updated equipotential shapes of Jupiter and Saturn using Juno and Cassini grand finale gravity science measurements. *Journal of Geophysical Research: Planets*, *125*, e2019JE006354. https://doi.org/10.1029/2019JE006354

Received 21 JAN 2020
Accepted 28 JUL 2020
Accepted article online 4 AUG 2020

Abstract A commonly used shape model for the giant plants of Jupiter and Saturn is an oblate ellipsoid, a simplified model of the equipotential shape. The ellipsoidal shape models were originally derived from radio occultation data and gravity data after the Voyager flybys in 1979. Through precise Doppler tracking of NASA's Juno and Cassini spacecraft telecommunications links, zonal coefficients in a spherical harmonic expansion of the gravity field of Jupiter and Saturn have been resolved to degree 10, including the detection of nonzero odd zonal harmonics, which have been interpreted as differential rotation in the atmosphere for both planets. In this work, we construct the equipotential surfaces of Jupiter and Saturn using the recently measured gravity fields determined by Juno through perijove 8 and Cassini through end of mission. For both planets, even zonal harmonics dominate the equipotential shape, differing from the reference ellipsoid up to ~32 km at Jupiter and ~125 km at Saturn in the midlatitude regions. Saturn's internal rotation period estimated with ring seismology produces a shape that is fully consistent with the Pioneer and Voyager radio occultation measurements, and Jupiter's shape is fully consistent with the Pioneer and Voyager radio occultation measurements. With current equipotential theory, the recent analysis of the depth of the deep zonal flow on Jupiter and Saturn cannot fully be explained by the shape from current radio occultation measurements; additional occultation measurements and reanalysis of the Pioneer and Voyager radio occultations and will be useful for further constraining the shape of the planets.

Plain Language Summary The standard shape of Jupiter and Saturn is often described assuming a flattened ellipsoid. The shapes were derived by data collected from the Voyager spacecraft in 1979. Juno has measured the gravity field of Jupiter to unprecedented precision, and Cassini has measured the gravity field of Saturn during the Grand Finale and internal rotation rate of Saturn with ring seismology. We use these updated data to infer equipotential shape models of the gas giant planets which can be applied to interior modeling and radio occultation analysis.

1. Introduction

The physical shape of a gas giant planet corresponds with the radius of a given pressure level with respect to the planet's center, commonly the 1-bar pressure level. The planet's physical shape is affected by the planet's zonal gravitational harmonics and centrifugal potential (Kaula, 1966) and is therefore affected by the rotation rate and atmospheric winds. While knowledge of the continuous shape of a planet (i.e., radius vs. latitude) is available, structure models typically consider only the oblateness (flattening) or average radius of the planet. The exact planetary shape indeed has only a limited effect on interior models (Helled & Guillot, 2013). However, the measured shape can be used to determine the planetary rotation rate and to identify the contribution of the zonal winds to the shape (Helled et al., 2009; Helled, 2011) and is required for analysis of radio occultation measurements (Lindal et al., 1985).

Jupiter's shape is commonly represented as be an ellipsoid with a 1-bar equatorial radius (A) of 71,492 ($\pm$4) km and polar radius (B=C) of 66,854 ($\pm$10) km. Similarly, Saturn's 1-bar shape is presented as an ellipsoid with an equatorial radius of 60,268 ($\pm$4) km and polar radius of 54,364 ($\pm$10) km. Both shapes are adopted by the International Astronomical Union (IAU) primarily for cartographic purposes (Archinal et al., 2018) and do not accurately describe midlatitude shape data. The equatorial and polar radii were derived based

upon a least squares fit of the Voyager and Pioneer radio occultations to the best-known equipotential shape at the time (Lindal et al., 1981, 1985; Lindal, 1992).

There are several ways to measure the shapes of planets. Two commonly used techniques in planetary probe exploration are imaging or radio occultations. In the case of giant planets, comparing the isobaric shape measured with these techniques with the theoretical equipotential shape, one can gain information on the higher-order gravity field, differential rotation from the departure from rotation on cylinders, and departure from barotropic structure. The physical shape of Jupiter can be used to constrain the solid body rotation and the depth of the winds (assuming differential rotation on cylinders).

The equipotential shape relies on the knowledge of the zonal harmonics of the planetary body. The zonal harmonics are the azimuthally symmetric components of the spherical harmonic expansion of the gravitational potential. Prior to the arrival of Juno at Jupiter and Cassini at Saturn, the best estimate of the gravitational fields came primarily from measurements taken during the Pioneer and Voyager flybys (Campbell & Synnott, 1985; Campbell & Anderson, 1989). The gravitational fields were refined over time using additional spacecraft and ground observations jointly with estimation of the system ephemeris (Jacobson, 2003; Jacobson et al., 2006). With Juno's arrival at Jupiter in 2016, the knowledge of the gravitational field was improved by a factor of five from the first two orbits alone (Folkner et al., 2017) and a factor of ~100 with the addition of three more orbits (Iess et al., 2018), affording the first detection of odd zonal harmonics.

Juno's gravity measurements may allow constraints to be placed on the depth of the zonal winds. Interpretations of the zonal harmonics as differential rotation by Kaspi et al. (2018) showed that the odd zonal harmonics are consistent with surface-measured zonal winds penetrating to a depth of ~3,000 km (exponential scale height). This was verified by analyzing the even zonal harmonics which found that the differential rotation is suppressed between a depth of 2,000 to 3,500 km (Guillot et al., 2018). Kong et al. (2018) discussed the nonuniqueness of this interpretation by showing that the zonal gravity harmonics can also be fitted with internal structure models which constrain the winds only to a shallow surface layer with appropriately derived deep zonal flows. Separately, Cassini's Grand Finale set of 22 orbits in 2017 provided unprecedented accuracy on the gravitational field of Saturn, where large differential rotation produces amplified higher-order even zonal harmonic coefficients (Iess et al., 2019; Galanti et al., 2019). For Saturn, the depth of the winds is estimated to be ~9,000 km. Both of these estimates are in excellent agreement with the prediction of Liu et al. (2008) based on the expected induced ohmic dissipation. However, Qin et al. (2020) derive a fit to the Saturn gravity field with a zonal circulation 20,000 km deep and confining the zonal winds to a weather layer on the surface.

Jupiter's rotation rate has been determined to high precision thanks to decades of radio astronomy measurements to be 9 hr 55 min 29.71 s (Dessler, 1983); this rate is generally assumed to be the internal rotation period of the planet. Higgins et al. (1997) suggested that this rotation rate could differ by 0.025 s, but magnetic field data from Galileo did not substantiate this claim (Russell et al., 2001). Using pre-Juno data, it was shown that Jupiter's measured shape is consistent with its measured System III rotation period and observed winds at latitudes between 20 and 30 degrees are consistent with differential rotation on cylinders between 20 and 30 degrees (Helled, 2011).

Saturn's internal rotation period is still not as well-determined as Jupiter's despite years of research on the subject. For a while Saturn's internal rotation period was assumed to be 10 hr 39 min 24 s as suggested by magnetic field and kilometric radiation measurements from the Voyager spacecraft (Desch & Kaiser, 1981). However, the kilometric radiation is modulated by as much 1% over timescales of years and slips with respect to the internal rotation period of Saturn (Gurnett et al., 2007). The magnetic rotation does not match the shape of Saturn as originally demonstrated previously by Anderson and Schubert (2007) and Helled et al. (2009) further suggesting that the internal rotation rate must be different than that was measured from the magnetic field and kilometric radiation. A more promising measure of the internal rotation period was found using the technique of ring seismology to be 10 hr 33 min 38 s (Mankovich et al., 2019), which matches within error bars of previous estimates from radio occultation data of 10 hr 32 min 35 s (Helled et al., 2009), potential vorticity of 10 hr 34 min 13 s (Read et al., 2009), and gravity and shape data of 10 hr 32 min 45 s (Helled et al., 2015).

In this work, we use the updated knowledge of Jupiter and Saturn's zonal harmonics (Iess et al., 2018, 2019), known and measured rotation rates of the planets, surface wind profile as measured by Cassini (García-Melendo et al., 2011; Porco et al., 2003) to compute an updated equipotential shape model and compare against gravity fields prior to the arrival of Juno and Cassini's Grand Finale. Various iterations of the equipotential shape are compared to determine the dominant zonal harmonics, the effect of the odd zonal harmonics on the shape, and the effect of deeply penetrating zonal winds on the shape. We recommend and provide the shape models computed in this work in the form of a Digital Shape Kernel (DSK) file, a standard kernel built-in with the Navigation and Ancillary Information Facility (NAIF) SPICE toolkit (Acton et al., 2018) suggested for standard distribution and application of equipotential shape models for giant planets.

2. Equipotential Shape Modeling

Provided that certain conditions are met, one can define an equipotential shape that coincides with a constant-pressure and constant-density surface. In this case, one can compute a local acceleration $\boldsymbol{g}$ by taking the gradient of a potential function:

$$\boldsymbol{g} = -\nabla U \tag{1}$$

The effective equipotential U of a planetary body in hydrostatic equilibrium is defined as the sum of the gravitational potential and the centrifugal potential Q:

$$U = \frac{GM}{r}\left(1 - \sum_{n=2}^{\infty}\left(\frac{a}{r}\right)^2 J_{2n} P_n(\sin\phi)\right) + Q \tag{2}$$

where GM is the gravitational parameter, r is the radius, a is the reference equatorial radius, J_n is the zonal harmonic coefficient of degree n, P_n is the Legendre polynomial of degree n, and φ is the geocentric latitude. The centrifugal potential Q is defined as the integral (e.g., Schinder et al., 2015):

$$Q = \int_0^R \omega^2 R dR \tag{3}$$

where R is the cylindrical radius and ω is the rotation rate, assumed to be a function of R only. For solid body rotation, that is, ω is a constant ω_0, this integral evaluates to the well-known result (using spherical coordinates, i.e., $R = r\cos\phi$):

$$Q = \frac{1}{2}\omega_0^2 r^2\left(1 - \sin^2\phi\right) \tag{4}$$

The equipotential surface with solid body rotation does not correspond with the isobaric surface in the presence of zonal winds. The zonal winds cause small perturbations in the rotation rate in the outer part of the planet, and thus, the centrifugal potential Q must be evaluated based on a wind model. Lindal et al. (1985) provide detailed geodetic calculations for the effect of the zonal winds, and a summary of those calculations follows with minor changes to the notation. In the presence of a zonal wind field with velocity V_W, the rotation is perturbed by

$$\omega = \omega_0 + \frac{V_W}{r\cos\phi} \tag{5}$$

Here it is assumed that the zonal wind velocity is a function of latitude only and not radius. This implies that the zonal winds rotate on cylinders penetrating deeper into the planet than the region probed by occultation. Lindal et al. (1985) then demonstrate that the relationship between local gravity and the dynamical height can be expressed by evaluating line integrals on the gravity field lines:

$$\int_{\phi}^{\frac{\pi}{2}} \Delta g_W \sin\left(\phi + \psi_{ref}\right)\frac{r_{ref}(\phi)}{\cos\psi_{ref}} d\phi = \int_0^{h(\phi)} |\boldsymbol{g}| dh \tag{6}$$

where $h(\varphi)$ is the dynamical height caused by the zonal winds, r_{ref} is the reference radius of the equipotential surface, and the angle ψ_{ref} is the difference between planetocentric and planetographic latitude

(as defined by the reference equipotential surface). The local gravity g is perturbed by the zonal winds by an amount Δg_W:

$$\Delta g_W = V_W \left[2\omega_0 + \frac{V_W}{r\cos\phi} \right] \tag{7}$$

By combining Equations 6 and 7, and solving for h, the dynamical heights h from zonal winds can be shown to be

$$h(\phi) = \frac{1}{g_{avg}} \int_{\phi}^{\frac{\pi}{2}} V_W \left(2\omega_0 + \frac{V_W}{r_{ref}(\phi)\cos\phi} \right) \frac{\sin\left(\phi + \psi_{ref}\right)}{\cos\left(\psi_{ref}\right)} r_{ref}(\phi) d\phi \tag{8}$$

where g_{avg} is the average acceleration due to gravity between the nominal equipotential surface and the one perturbed by the dynamical height. To solve for the equipotential surface, a constant equipotential U_0 is computed at a reference radius r_0 at a given latitude φ_0. For each latitude, Newton-Raphson iteration is applied to numerically solve for a radius r in which the equipotential U equals the constant equipotential U_0 as defined at the reference radius and latitude. The dynamical heights $h(\varphi)$, if applicable, are then added to the equipotential to compute the isobaric surface.

The use of zonal wind profiles to calculate the equipotential surface makes several assumptions. Importantly, occultation data measure the shape of the isopycnic surfaces, while the dynamical height equations in Lindal et al. (1985) yield the height of the isobars. For these shapes to coincide, the relevant atmospheric region must be barotropic, and indeed an equipotential surface can only be calculated with the help of Equation 2 if this is true. The derivation of Equation 8, discussed in the Appendix of Lindal et al. (1985), assumes that the winds do not vary with altitude. For applicability to Jupiter and Saturn, this would imply that the winds would need to penetrate very deep. Interpretations of the zonal harmonics at Jupiter (Guillot et al., 2018; Kaspi et al., 2018) and Saturn (Iess et al., 2019, Galanti et al., 2019) show that the measured zonal harmonics can be explained if the observed surface zonal winds penetrate to depths of 3,000 km for Jupiter and 9,000 km for Saturn (exponential scale heights). The decay heights are consistent with the ohmic dissipation constraints (Liu et al., 2008) and for the case of Jupiter is supported both by the even and odd harmonics and are also supported by magnetic data (Galanti et al., 2017). This interpretation is nonunique, as the zonal winds may be confined to a thin weather layer on the surface (Kong et al., 2018; Qin et al., 2020). Thus, it remains to be determined if the variation of the flows with depth is comparable with the observed atmospheric winds (e.g., Duer et al., 2019). This has implications on the applicability of Equation 8: If the winds penetrate deeply into the interior, then the assumption of the same surface zonal winds rotating with the planet on cylinders may be more applicable than if the zonal winds are confined to the surface or differ from zonal flows at depth.

The wind velocities are measured by cloud tracking (Limaye, 1986; García-Melendo et al., 2011) relative to an assumed rotation period. This is typically at a given pressure level corresponding with the clouds. It would be expected that the isobaric shape is expected to change at different pressure levels due to the effect of the winds. Prior to Juno and Cassini grand finale, it was difficult to assume the depth of the zonal winds; therefore Equation 8 requires that the winds penetrate to the interior and that the planet is rotating on cylinders. Differences in the assumed rotation period from the actual rotation period would affect the relative magnitude of the wind velocities and thus the shape as well.

3. Results

The updated equipotential surface using the latest gravitational field coefficients is shown in Figure 1. Two equipotential shapes were computed for each planet. The first shape simply uses the equipotential without consideration of the zonal winds assuming the spin period is 9 hr 55 min 29.7 s for Jupiter (Lindal, 1992) and 10 hr 33 min 38 s (uncertainties of −1 min 19 s, +1 min 52 s) for Saturn based on the most recent ring seismology estimate (Mankovich et al., 2019). Jupiter's shape is fully consistent with Kong et al. (2016). The second shape considers the dynamical height effect of the zonal winds using Equation 4 using the zonal wind profiles from Cassini (García-Melendo et al., 2011; Porco et al., 2003). For both planets, the polar radius is

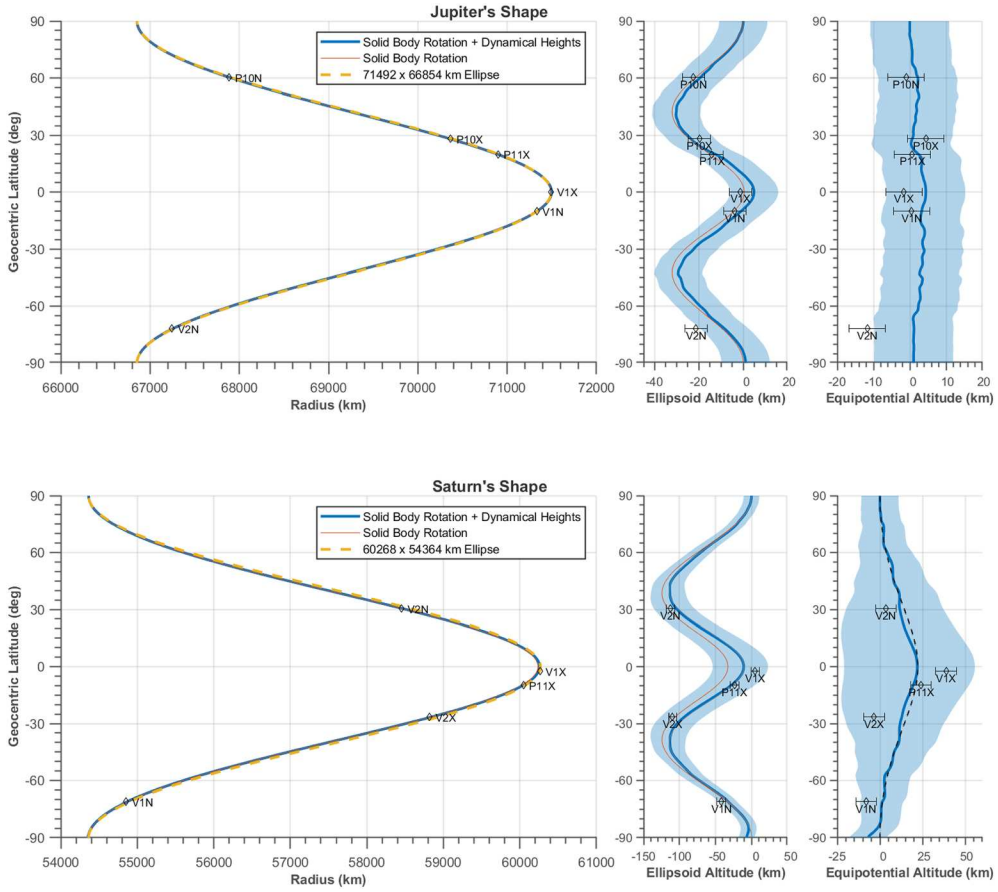

Figure 1. The 1-bar equipotential surface of Jupiter (top) and Saturn (bottom) as a function of latitude. The left panels show the overall shape, dominated by the ellipsoidal flattening. The middle panels show the equipotential surface difference from the reference ellipsoid with (bold blue line) and without (narrow orange line) the contribution of zonal winds. The right panels show the difference from the solid body equipotential surface without winds. The uncertainty in the model is shown with shaded blue regions, computed by the root-sum-square of the mapped uncertainties in the shape, primarily: The polar reference radius (10 km), zonal winds (3–4 km), and for Saturn, the internal rotation rate (<2 min). The radio occultation 1-bar radii, marked with the occultation identification number, are overlaid for comparison (radio occultation errors are ~5 km for Jupiter and ~6 km for Saturn). Occultations are identified by the spacecraft (V1 is Voyager 1, V2 is Voyager 2. P10 is Pioneer 10, P11 is Pioneer 11) and occultation type (X is egress, N is ingress). A tabulated version of these data is provided in the accompanying data set (Buccino, 2020).

held fixed as the reference radius (at the 1-bar pressure level: Jupiter, $B = 66{,}854$ km, Saturn $B = 54{,}364$ km). Although the equatorial radius is better known (±4 km) than the polar radius (±10 km), the dynamical heights are largest at the equatorial region and do not affect the pole.

The equipotentials are compared against the measured 1-bar occultation radii (Lindal et al., 1981, 1985) as digitized by Helled et al. (2009). As of this time and to the best of our knowledge, no radio occultation radii from Cassini have been published or archived. The measurement uncertainty in the Jupiter radio occultation measurements is approximately ~5 km (Lindal et al., 1981). The measurement uncertainty of Saturn radio occultation measurements is not given in the original literature (Lindal et al., 1985), but Cassini's yet unpublished radio occultation measurements have an uncertainty of ~6 km (Flasar et al., 2013), which we adopt for this work. The actual uncertainty in the Saturn occultation radii is likely larger, due to both modeling the differential rotation and due to the larger navigation uncertainties in the positions of the Pioneer and Voyager spacecraft at the time of the occultation analysis in the 1980s.

On Jupiter, the equipotential surface differs from the reference ellipse by 37 km at midlatitude regions (±40°). The zonal winds perturb the shape by several kilometers. This has an effect that the polar regions are slightly drawn in by ~5 km. These results are consistent with the 5 km inferred by Helled et al. (2009)

Table 1
Effect of Gravitational Zonal Harmonics on the Equipotential Shape

	Jupiter		Saturn	
Gravity coefficients	Δr_{max} reference ellipse	Δr_{max} updated equipotential	Δr_{max} reference ellipse	Δr_{max} updated equipotential
J_2–J_{10}[a] (this work)	32.4 km	0 km	125 km	0 km
Jacobson J_2, J_4, J_6[b]	32.4 km	0.19 km	124 km	1.9 km
Pioneer/Voyager J_2, J_4, J_6[c]	34.4 km	4.3 km	118 km	7.1 km
J_2[a]	35.8 km	37.29 km	39 km	116 km
J_2, J_4[a]	31.9 km	4.1 km	134 km	12.9 km
J_2, J_4, J_6[a]	32.4 km	0.2 km	124 km	1.9 km
J_2, J_4, J_6, J_8[a]	32.4 km	0.04 km	125 km	1.0 km
J_2, J_4, J_6, J_8, J_{10}[a]	32.4 km	0.01 km	125 km	0.1 km

Note. For each planet, the left column is the maximum radius difference between the computed equipotential surface and the reference ellipse, and the right column is the maximum radius difference between the computed equipotential surface and the updated reference equipotential surface (first row, using the full set of the J_2–J_{10} coefficients). Dynamic heights are not considered in this table.
[a]Jupiter from Iess et al. (2018); Saturn from Iess et al. (2019). [b]Jupiter from Jacobson (2003); Saturn from Jacobson et al. (2006). [c]Jupiter from Campbell and Synnott (1985); Saturn from Campbell and Anderson (1989).

and imply that the zonal winds have negligible contribution to Jupiter's physical shape. The uncertainties in the shape are dominated by the uncertainty in the reference radius (4–10 km, depending on if the polar radius or equatorial radius was chosen), which is on the same order of the zonal winds. The occultation data are consistent within error bars of the shape. The Voyager 2 egress occultation (V2N) at −71 degrees latitude is the least consistent; this could be due to an unmodeled physical phenomenon in the North-South asymmetry of the planet or a larger measurement uncertainty due to the geometry of the occultation itself.

On Saturn, the equipotential surface using the rotation rate from ring seismology (Mankovich et al., 2019) differs more significantly from the reference ellipse, by 125 km at midlatitude regions and 32 km at the equator. Saturn's strong zonal winds perturb the shape by 21 km at the equator and bring the shape closer to the reference ellipse, though a majority of this correction could also come by ignoring the dynamical heights and adjusting the rotation rate by −1 min 17 s, within the error bars of the ring seismology measurement. The uncertainty in the rotation rate as measured by ring seismology and polar radius imply the uncertainty in the shape of Saturn at the equator is ~80 km. All occultation radii measurements are fully consistent within the error bars for Saturn.

3.1. Effect of Gravitational Harmonics

By assuming solid body rotation (i.e., no dynamical heights) with various combinations of gravitational coefficients, the impact each coefficient has on the equipotential surface can be determined (Table 1). In addition, equipotential surfaces are computed with previous gravity solutions, prior to the arrival of Juno or Cassini's Grand Finale orbits for comparison.

For Jupiter, aside from the ellipsoidal effect of the J_2 coefficient, the J_4 coefficient has the largest effect, pulling the equipotential surface inward at midlatitude regions by ~37 km. The corresponding J_6 effect is an order of magnitude smaller at ~4 km. The J_8 and J_{10} coefficients have a very small effect on the shape, less than 1 km. If the odd zonal harmonics, J_3, J_5, J_7, and J_9 are to affect the shape; combined they have a very small effect, even smaller than the effect of J_8.

The effect is similar for Saturn but is much more profound. The J_4 coefficient pulls in the surface by 116 km at midlatitude regions. Each coefficient has a correspondingly smaller effect, about an order of magnitude per degree. The odd zonal harmonics and the J_{10} coefficient have subkilometer impacts on the equipotential shape.

To evaluate the impact of the updated equipotential surface, the equipotential was compared using all the well-determined zonal coefficients from Juno (J_2–J_{10}) (Iess et al., 2018) and Cassini's Grand Finale (Iess et al., 2019) against the equipotential using all the well-determined coefficients during the Voyager-era (J_2, J_4, J_6) (Campbell & Synnott, 1985; Campbell & Anderson, 1989) and from orbital tours (Galileo-era for

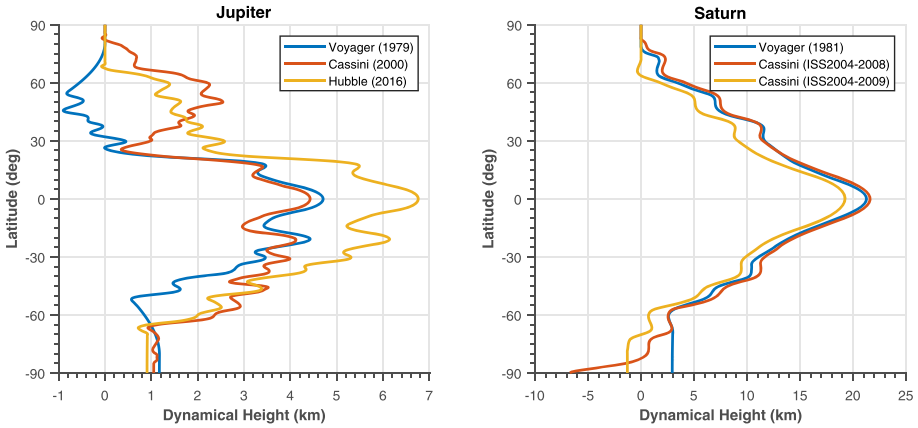

Figure 2. The dynamical height offset of the isobaric surface from the equipotential surface of Jupiter (left) and Saturn (right). The reference radius of 0 km is the equipotential shape of the planet derived from the zonal gravitational harmonics assuming solid body rotation only. Dynamical heights generated from different measured zonal wind profiles are plotted; the maximum difference in shape between zonal wind models on Jupiter is ~3 km and on Saturn is ~4 km.

Jupiter, Jacobson, 2003; and Cassini prime mission, Jacobson et al., 2006). The difference in equipotential surfaces is on the order of several kilometers between Voyager-era and this solution (~4 km for Jupiter, ~7 km for Saturn). The orbital tour gravity solutions provide equipotential surfaces which better match this solution (<1 km for Jupiter, <2 km for Saturn).

3.2. Effect of Zonal Winds

The calculation of the isobaric surface relies on knowledge of the zonal wind profile, which perturbs the rotation rate of the fluid near the surface. The first high-precision measurement of Jupiter's zonal wind profile was taken by the Voyager imaging subsystem instrument during the flybys of Voyager 1 and 2 in 1979 (Limaye, 1986). When Cassini flew by Jupiter in 2000, it performed an extensive survey of the Jovian system, including measurement of the zonal winds (Porco et al., 2003). More recently, estimates of the zonal wind profile with the Hubble Space telescope have been made (Tollefson et al., 2017). The Voyager spacecraft measured Saturn's strong zonal wind profile in 1981 (Sanchez-Lavega et al., 2000). Cassini's imaging subsystem has also measured the zonal wind profile of Saturn during its orbital tour (García-Melendo et al., 2011).

To understand the sensitivities to the zonal wind profile used in the computation of the shape of Jupiter and Saturn, the dynamical heights are computed using Equation 4 with several published zonal wind models as described above. The resulting dynamical heights are shown in Figure 2. For Jupiter, the dynamical height differences between various zonal wind models peak at ~3 km. This difference is most prevalent between Voyager and Cassini zonal wind profiles in the midlatitude regions of the northern hemisphere (40–60° N). Although the Voyager and Cassini zonal wind profiles agree near the equatorial region well, they differ significantly by 2–3 km from Hubble measurements in 2018 (Simon et al., 2015). For Saturn, the dynamical height contribution to the shape using Voyager and Cassini ISS2004-2008 zonal wind profiles agree fairly well (the two Cassini wind zonal wind profiles are defined in García-Melendo et al., 2011). Interestingly, the ISS2004-2009 zonal wind profile is offset from the ISS2004-2008 model by ~2 km.

Despite the small differences this analysis confirms that the wind velocities and the wind structure of both Jupiter and Saturn are stable on timescales of tens of years. This also means that the results of structure models that include the effect of dynamics are not affected by the choice of the used wind data (Guillot et al., 2018; Iess et al., 2019).

3.3. Surface Gravity

The elliptical nature of the planets causes deviations in gravitational acceleration between the pole and the equator, as expected and shown in Figure 3. On Jupiter, the gravitational acceleration at the 1-bar surface at the poles is 27.02 m/s^2 and at the equator is 23.15 m/s^2. The direction vector of the gravitational acceleration on the surface differs from an ellipsoidal approximation by 0.06 degrees in midlatitude regions where the gradient of the equipotential shape is most different from an ellipsoid (Figure 1). For Saturn, to compute

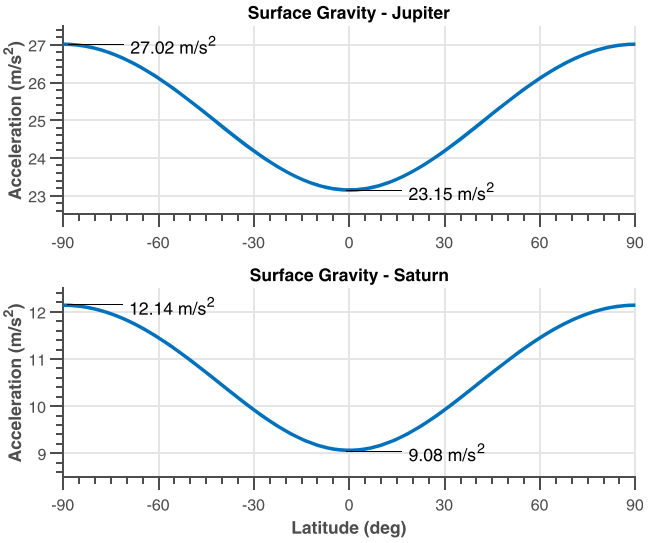

Figure 3. Radial gravity acceleration on the 1-bar equipotential for Jupiter (top) and Saturn (bottom), derived from the zonal gravitational harmonics assuming solid body rotation only. For Saturn, the rotation rate from ring seismology is assumed to be 10 hr 33 min 38 s (Mankovich et al., 2019).

the surface accelerations, a rotation rate from ring seismology of 10 hr 33 min 38 s is assumed (Mankovich et al., 2019). The gravitational acceleration at the 1-bar surface at the poles is 12.14 m/s^2 and at the equator is 9.08 m/s^2. The direction vector of the gravitational acceleration differs from the ellipsoidal by 0.24 degrees, again in mid-latitude regions. If the contribution of zonal winds is considered, the equatorial surface acceleration decreases by 0.01% for Jupiter and 0.1% for Saturn.

3.4. Use of Equipotential Shapes Beyond Interior Modeling

Nonellipsoidal shapes are commonplace throughout multiple solar system objects but not typically used widely for Jupiter and Saturn. Approximations of the shape of the planets are useful for applications outside interior modeling. One example is the computation of surface normals and phase angles, which are important inputs for calculating emittance. Another application is occultation geometry and limb fitting, which can be used in the determination of radius measurements of the surface itself. To this end, we provide an accompanying data set with this paper containing the shape models evaluated in formats usable in common formats.

The Navigation and Ancillary Information Facility (NAIF) is a node of the Planetary Data System (PDS) which archives mission geometry information. NAIF maintains the SPICE toolkit (Acton et al., 2018) which has built-in algorithms to do precisely these types of calculations. SPICE, as a long existing software tool in the planetary community, is integrated into software sets such as ISIS for image processing (Gaddis et al., 1997). The Digital Shape Kernel (DSK) is a recent addition to the SPICE toolkit which provides a method to interface SPICE geometric functions with arbitrary-shape planetary bodies (Bachman, 2017).

A DSK contains spatial position of discreet plates which define a surface. To use a DSK on a planet of Jupiter-scale, it is crucial to understand the discretization of the equipotential surface into plates. If we assume that each plate is a square of equal longitude and geocentric latitude, the discretization error is a simple function of the radius of the planet and the angular spacing of the plates. To achieve subkilometer discretization error at the equator, 0.5-degree plate spacing is required. A minimum discretization error of ~0.15 km is possible within these limits but is not needed due to the larger uncertainty in the shape itself.

The use of a DSK allows the end-user, who may not be familiar with spherical harmonics, the ability to evaluate the shape through a simple user interface in any coordinate system that can be defined within the SPICE system. We provide the equipotential shape models derived in this work as tabulated plain-text files and DSKs in 0.5-degree resolution on the NASA Open Data portal (Buccino, 2020).

4. Discussion

Over the last several years, the Juno and Cassini spacecraft have made high precision measurements of the gravitational field of Jupiter and Saturn and along with ground-based observations from Hubble have exquisitely mapped the zonal wind profiles on the planets. Table 2 discusses the uncertainties associated with each component that derives the shape with the method used in this paper.

Juno's measurements of the gravitational field (Iess et al., 2018) are ~100 times more precise than Pioneer/Voyager and as such have reduced the mapped uncertainty in the equipotential on the order of ~100× as well, down to 0.01 km (primarily driven by the uncertainty in the J_{10} coefficient).

The mapped uncertainty from the zonal winds comes primarily from the changes in the zonal flows over time. Between the 1979 Voyager flyby and the 2000 Cassini flyby of Jupiter, changes in the zonal flows are up to ~45 m/s. The physical measurement error of the zonal flows from image cross-correlation is much smaller, for example, peaking at ~1.5 m/s from the Voyager estimates of the zonal flow (Limaye, 1986). Similarly, for Saturn the measured zonal wind profile differs between the Voyager flyby and Cassini's

Table 2
Uncertainty in Jupiter and Saturn's Equipotentials, Divided Into the Individual Sources

	Jupiter		Saturn	
Parameter	Parameter uncertainty	Mapped shape uncertainty	Parameter uncertainty	Mapped shape uncertainty
J_2[a]	0.014	0.0016 km	0.028	0.0036 km
J_3[a]	0.01	0.0009 km	0.023	0.0036 km
J_4[a]	0.004	0.0003 km	0.037	0.0049 km
J_5[a]	0.008	0.0008 km	0.054	0.010 km
J_6[a]	0.009	0.0011 km	0.087	0.014 km
J_7[a]	0.017	0.0019 km	0.112	0.026 km
J_8[a]	0.025	0.0026 km	0.205	0.039 km
J_9[a]	0.044	0.0057 km	0.260	0.076 km
J_{10}[a]	0.069	0.01 km	0.420	0.1 km
ω	0.025 s[b]	0.004 km	<2 min[c]	80 km
Reference radius	4–10 km[d]	4–10 km	4–10 km[d]	4–10 km
Zonal winds	ΔV_0–45 m/s	3 km	ΔV_0–100 m/s	4.3 km

[a]3-sigma uncertainty in the gravitational harmonics from Iess et al. (2018) (Jupiter) and Iess et al. (2019) (Saturn). [b]Russell et al. (2001) suggest that Jupiter's rotation rate may differ from system III by 0.025 s. [c]Mankovich et al. (2019) states the uncertainty is −1 min 19 s, +1 min 52 s. [d]Radius uncertainty from Lindal (1992).

orbital tour of Saturn are ~100 m/s in the equatorial region (García-Melendo et al., 2011). The difference in the shape is quantified by differencing the dynamical heights computed with Voyager and Cassini zonal wind profiles and maps to a ~3 km shape uncertainty for Jupiter and ~4.3 km shape uncertainty for Saturn.

The corresponding difference in the shape with the Voyager rotation period is ~120 km, consistent with previous studies. As a result, a larger uncertainty of Saturn's shape should be considered in Saturn structure models (e.g., Helled & Guillot, 2013).

By comparing radio occultation radius measurements to the equipotential shape, it is possible to gain information on the zonal coefficients of the gravity field, the spin rate of the planet, and the magnitude of the dynamical heights. Radio range-rate measurements have determined the zonal coefficients to high precision (Iess et al., 2018, 2019), so radio occultation measurements will not be able improve those any further. In the case of Saturn's uncertain rotation rate, Helled et al. (2015, 2009) showed that Saturn's rotation rate could be measured from the shape, and the estimate has been consistent with the newer estimate from ring seismology (Mankovich et al., 2019). By measuring the dynamical heights, one can answer questions about departure of the planet from rotation on cylinders or a departure from a barotropic structure in the atmosphere. Addressing these questions in relation to the dynamical heights will come down to how accurately the dynamical heights can be measured.

In the case of Jupiter, the uncertainty of the equipotential shape (~10 km) is dominated by the reference radius and is on-par with the accuracy of the radio occultation measurements (~5 km). This is also on the same order of magnitude of the dynamical height contribution (<7 km), assuming that the observed zonal wind field acts as rotation on cylinders into the interior of the planet. The changes in dynamical height with different zonal wind profiles (<3 km) are also smaller than this uncertainty. Thus, with the current state, it is difficult to confirm that the dynamical heights significantly contribute to Jupiter's shape. Reducing the uncertainty in the reference radius may help further constrain this problem.

In their analysis of the Voyager radio occultations of Jupiter, Lindal et al. (1981) discuss that the two major sources of uncertainty in the determination of the altitude of the isobaric surface are uncertainties in the spacecraft trajectory and the uncertainty in the shape of the equipotential surface. The uncertainty of the J_6 coefficient, at the time, mapped into a 5 km polar radius uncertainty. Since the analysis of radio occultations relies on the knowledge of the isobaric surface, a reanalysis of the Voyager radio occultations in light of the Juno gravitational field measurements may help in reducing the uncertainty in the reference radius.

It is still to be determined whether an improved knowledge of the reference radius can be used to constrain the depth of the zonal winds and the interplay between the two. Kaspi et al. (2018) explained the odd gravity

harmonics by allowing the zonal winds penetrate to 3,000 km depth, in which case the dynamical height estimation from Lindal et al. (1985) may be applicable to some extent. This is complicated by the variation in the observed zonal wind field of ~3 km (Figure 2). However, Kong et al. (2018) were able to explain Juno's gravity measurements with an alternate deep zonal flow profile, keeping the zonal winds themselves confined to a thin weather layer. Only five radio occultations exist and are sparsely spaced out in longitude, further constraining the ability to discern a zonal profile from shape measurements; more occultation measurements may help solve this.

To summarize, we suggest that the shape of giant planets reveal information on their centrifugal potential and therefore on their atmosphere dynamics and rotation periods. This information can then be used by internal structure models. More information on Saturn's shape is expected from Cassini data that are still being processed. For Jupiter, occultation measurements are planned for the ESA JUICE mission. This information can then be applied in the future to further study the gas giants of our planetary system.

Data Availability Statement

The gravitational field coefficients used in this work are published in Iess et al. (2018) and Iess et al. (2019). Zonal wind profiles used for the dynamical heights are published in Limaye (1986), Porco et al. (2003), Tollefson et al. (2017), Sanchez-Lavega et al. (2000), and García-Melendo et al. (2011). The equipotential shapes of Jupiter and Saturn produced in this work are archived in NASA Open Data Portal (Buccino, 2020).

Acknowledgments

This work was partially carried out at the Jet Propulsion Laboratory, California Institute of Technology, under contract with the National Aeronautics and Space Administration. Government sponsorship acknowledged. R. H. acknowledges support from SNSF grant 200020_188460. Finally, we thank the Juno science team members for valuable discussions.

References

Acton, C., Bachman, N., Semenov, B., & Wright, E. (2018). A look towards the future in the handling of space science mission geometry. *Planetary and Space Science*, *150*, 9–12. https://doi.org/10.1016/j.pss.2017.02.013

Anderson, J. D., & Schubert, G. (2007). Saturn's gravitational field, internal rotation, and interior structure. *Science*, *317*(5843), 1384–1387. https://doi.org/10.1126/science.1144835

Archinal, B. A., Acton, C. H., A'Hearn, M. F., Conrad, A., Consolmagno, G. J., Duxbury, T., et al. (2018). Report of the IAU working group on cartographic coordinates and rotational elements: 2015. *Celestial Mechanics and Dynamical Astronomy*, *130*(3), 22. https://doi.org/10.1007/s10569-017-9805-5

Bachman, N. J. (2017, June). The SPICE digital shape kernel (DSK) subsystem. In Third Planetary Data Workshop and The Planetary Geologic Mappers Annual Meeting (Vol. 1986). https://www.hou.usra.edu/meetings/planetdata2017/pdf/7015.pdf

Buccino, D. (2020). Equipotential shape models for the gas giants [data set], NASA Open Data Portal, https://doi.org/10.25966/4S3C-RW61

Campbell, J. K., & Anderson, J. D. (1989). Gravity field of the Saturnian system from Pioneer and voyager tracking data. *The Astronomical Journal*, *97*, 1485–1495. https://doi.org/10.1086/115088

Campbell, J. K., & Synnott, S. P. (1985). Gravity field of the Jovian system from Pioneer and voyager tracking data. *The Astronomical Journal*, *90*, 364–372. https://doi.org/10.1086/113741

Desch, M. D., & Kaiser, M. L. (1981). Voyager measurement of the rotation period of Saturn's magnetic field. *Geophysical Research Letters*, *8*(3), 253–256. https://doi.org/10.1029/GL008i003p00253

Dessler, A. J. (1983). Coordinate systems. *Physics of the Jovian magnetosphere*, 498–504. https://doi.org/10.1017/CBO9780511564574.016

Duer, K., Galanti, E., & Kaspi, Y. (2019). Analysis of Jupiter's deep jets combining *Juno* gravity and time-varying magnetic field measurements. *The Astrophysical Journal Letters*, *879*, 2.

Flasar, F., Schinder, P. J., French, R. G., Marouf, E. A., & Kliore, A. J. (2013). Saturn's shape from Cassini radio occultations. AGUFM, 2013, P11B-08.

Folkner, W. M., Iess, L., Anderson, J. D., Asmar, S. W., Buccino, D. R., Durante, D., et al. (2017). Jupiter gravity field estimated from the first two Juno orbits. *Geophysical Research Letters*, *44*, 4694–4700. https://doi.org/10.1002/2017GL073140

Gaddis, L., Anderson, J., Becker, K., Becker, T., Cook, D., Edwards, K., et al. (1997). An overview of the integrated software for imaging spectrometers (ISIS). In Lunar and Planetary Science Conference (Vol. 28, p. 387).

Galanti, E., Cao, H., & Kaspi, Y. (2017). Constraining Jupiter's internal flows using Juno magnetic and gravity measurements. *Geophysical Research Letters*, *44*, 8173–8181. https://doi.org/10.1002/2017GL074903

Galanti, E., Kaspi, Y., Miguel, Y., Guillot, T., Durante, D., Racioppa, P., & Iess, L. (2019). Saturn's deep atmospheric flows revealed by the Cassini grand finale gravity measurements. *Geophysical Research Letters*, *46*, 616–624. https://doi.org/10.1029/2018GL078087

García-Melendo, E., Pérez-Hoyos, S., Sánchez-Lavega, A., & Hueso, R. (2011). Saturn's zonal wind profile in 2004–2009 from Cassini ISS images and its long-term variability. *Icarus*, *215*(1), 62–74. https://doi.org/10.1016/j.icarus.2011.07.005

Guillot, T., Miguel, Y., Militzer, B., Hubbard, W. B., Kaspi, Y., Galanti, E., et al. (2018). A suppression of differential rotation in Jupiter's deep interior. *Nature*, *555*(7695), 227–230. https://doi.org/10.1038/nature25775

Gurnett, D. A., Persoon, A. M., Kurth, W. S., Groene, J. B., Averkamp, T. F., Dougherty, M. K., & Southwood, D. J. (2007). The variable rotation period of the inner region of Saturn's plasma disk. *Science*, *316*(5823), 442–445. https://doi.org/10.1126/science.1138562

Helled, R. (2011). Jupiter's occultation radii: Implications for its internal dynamics. *Geophysical Research Letters*, *38*, L08204. https://doi.org/10.1029/2011GL047107

Helled, R., Galanti, E., & Kaspi, Y. (2015). A fast spinning Saturn determined from its gravitational field and oblateness. *Nature*, *520*(7546), 202–204. https://doi.org/10.1038/nature14278

Helled, R., & Guillot, T. (2013). Interior models of Saturn: Including the uncertainties in shape and rotation. *The Astrophysical Journal*, *767*(2), 113. https://doi.org/10.1088/0004-637X/767/2/113

Helled, R., Schubert, G., & Anderson, J. D. (2009). Jupiter and Saturn rotation periods. *Planetary and Space Science*, *57*(12), 1467–1473. https://doi.org/10.1016/j.pss.2009.07.008

Higgins, C. A., Carr, T. D., Reyes, F., Greenman, W. B., & Lebo, G. R. (1997). A redefinition of Jupiter's rotation period. *Journal of Geophysical Research*, *102*(A10), 22,033–22,041. https://doi.org/10.1029/97JA02090

Iess, L., Folkner, W. M., Durante, D., Parisi, M., Kaspi, Y., Galanti, E., et al. (2018). Measurement of Jupiter's asymmetric gravity field. *Nature*, *555*(7695), 220–222. https://doi.org/10.1038/nature25776

Iess, L., Militzer, B., Kaspi, Y., Nicholson, P., Durante, D., Racioppa, P., et al. (2019). Measurement and implications of Saturn's gravity field and ring mass. *Science*, *364*(6445), eaat2965. https://doi.org/10.1126/science.aat2965

Jacobson, R. A. (2003). Jupiter satellite ephemeris file Jup230. NASA Navigation and Ancillary Information Facility.

Jacobson, R. A., Antreasian, P. G., Bordi, J. J., Criddle, K. E., Ionasescu, R., Jones, J. B., et al. (2006). The gravity field of the Saturnian system from satellite observations and spacecraft tracking data. *The Astronomical Journal*, *132*(6), 2520–2526. https://doi.org/10.1086/508812

Kaspi, Y., Galanti, E., Hubbard, W. B., Stevenson, D. J., Bolton, S. J., Iess, L., et al. (2018). Jupiter's atmospheric jet streams extend thousands of kilometres deep. *Nature*, *555*(7695), 223–226. https://doi.org/10.1038/nature25793

Kaula, W. M. (1966). *Theory of Satellite Geodesy*. Waltham, Mass: Blaisdell Publ. Co.

Kong, D., Zhang, K., & Schubert, G. (2016). A fully self-consistent multi-layered model of Jupiter. *The Astrophysical Journal*, *826*(2), 127. https://doi.org/10.3847/0004-637X/826/2/127

Kong, D., Zhang, K., Schubert, G., & Anderson, J. D. (2018). Origin of Jupiter's cloud-level zonal winds remains a puzzle even after Juno. *Proceedings of the National Academy of Sciences*, *115*(34), 8499–8504. https://doi.org/10.1073/pnas.1805927115

Limaye, S. S. (1986). Jupiter: New estimates of the mean zonal flow at the cloud level. *Icarus*, *65*(2–3), 335–352. https://doi.org/10.1016/0019-1035(86)90142-9

Lindal, G. F. (1992). The atmosphere of Neptune-an analysis of radio occultation data acquired with voyager 2. *The Astronomical Journal*, *103*, 967–982. https://doi.org/10.1086/116119

Lindal, G. F., Sweetnam, D. N., & Eshleman, V. R. (1985). The atmosphere of Saturn—An analysis of the voyager radio occultation measurements. *The Astronomical Journal*, *90*, 1136–1146. https://doi.org/10.1086/113820

Lindal, G. F., Wood, G. E., Levy, G. S., Anderson, J. D., Sweetnam, D. N., Hotz, H. B., et al. (1981). The atmosphere of Jupiter: An analysis of the voyager radio occultation measurements. *Journal of Geophysical Research*, *86*(A10), 8721–8727. https://doi.org/10.1029/JA086iA10p08721

Liu, J., Goldreich, P. M., & Stevenson, D. J. (2008). Constraints on deep-seated zonal winds inside Jupiter and Saturn. *Icarus*, *196*(2), 653–664. https://doi.org/10.1016/j.icarus.2007.11.036

Mankovich, C., Marley, M. S., Fortney, J. J., & Movshovitz, N. (2019). Cassini ring seismology as a probe of Saturn's interior. I. Rigid rotation. *The Astrophysical Journal*, *871*(1), 1. https://doi.org/10.3847/1538-4357/aaf798

Porco, C. C., West, R. A., McEwen, A., del Genio, A., Ingersoll, A. P., Thomas, P., et al. (2003). Cassini imaging of Jupiter's atmosphere, satellites, and rings. *Science*, *299*(5612), 1541–1547. https://doi.org/10.1126/science.1079462

Qin, S., Kong, D., Zhang, K., Schubert, G., & Huang, Y. (2020). Interpreting the equatorially antisymmetric gravitational field of Saturn measured by the Cassini grand finale. *The Astrophysical Journal*, *890*(1), 26. https://doi.org/10.3847/1538-4357/ab6a9a

Read, P. L., Dowling, T. E., & Schubert, G. (2009). Saturn's rotation period from its atmospheric planetary-wave configuration. *Nature*, *460*(7255), 608–610. https://doi.org/10.1038/nature08194

Russell, C. T., Yu, Z. J., & Kivelson, M. G. (2001). The rotation period of Jupiter. *Geophysical Research Letters*, *28*(10), 1911–1912. https://doi.org/10.1029/2001GL012917

Sanchez-Lavega, A., Rojas, J. F., & Sada, P. V. (2000). Saturn's zonal winds at cloud level. *Icarus*, *147*(2), 405–420. https://doi.org/10.1006/icar.2000.6449

Schinder, P. J., Flasar, F. M., Marouf, E. A., French, R. G., Anabtawi, A., Barbinis, E., & Kliore, A. J. (2015). A numerical technique for two-way radio occultations by oblate axisymmetric atmospheres with zonal winds. *Radio Science*, *50*, 712–727. https://doi.org/10.1002/2015RS005690

Simon, A. A., Wong, M. H., & Orton, G. S. (2015). First results from the Hubble OPAL program: Jupiter in 2015. *The Astrophysical Journal*, *812*(1), 55. https://doi.org/10.1088/0004-637X/812/1/55

Tollefson, J., Wong, M. H., Pater, I., Simon, A. A., Orton, G. S., Rogers, J. H., et al. (2017). Changes in Jupiter's zonal wind profile preceding and during the Juno mission. *Icarus*, *296*, 163–178. https://doi.org/10.1016/j.icarus.2017.06.007